

# Relativistic Mean Field Model parameterizations in the light of GW170817, GW190814, and PSR J0740 + 6620

Virender Thakur,<sup>1,\*</sup> Raj Kumar,<sup>1,†</sup> Pankaj Kumar,<sup>1</sup> Vikesh Kumar,<sup>1</sup> B.K. Agrawal,<sup>2</sup> and Shashi K. Dhiman<sup>1,3,‡</sup>

<sup>1</sup>*Department of Physics, Himachal Pradesh University, Shimla-171005, India*

<sup>2</sup>*Saha Institute of Nuclear Physics, 1/AF Bidhannagar, Kolkata 700064, India*

<sup>3</sup>*School of Applied Sciences, Himachal Pradesh Technical University, Hamirpur-177001, India*

Three parameterizations DOPS1, DOPS2, and DOPS3 (named after the Department of Physics Shimla) of the Relativistic Mean Field (RMF) model have been proposed with the inclusion of all possible self and mixed interactions between the scalar-isoscalar ( $\sigma$ ), vector-isoscalar ( $\omega$ ) and vector-isovector ( $\rho$ ) mesons up to quartic order. The generated parameter sets are in harmony with the finite and bulk nuclear matter properties. A set of Equations of State (EOSs) composed of pure hadronic (nucleonic) matter and nucleonic with quark matter (hybrid EOSs) for superdense hadron-quark matter in  $\beta$ -equilibrium is obtained. The quark matter phase is calculated by using the three-flavor Nambu-Jona-Lasinio (NJL) model. The maximum mass of a non-rotating neutron star with DOPS1 parameterization is found to be around  $2.6 M_{\odot}$  for the pure nucleonic matter which satisfies the recent gravitational wave analysis of GW190814 [Abbott et al., *Astrophys. J. Lett.* **896**, L44 (2020)] with possible maximum mass constraint indicating that the secondary component of GW190814 could be a non-rotating heaviest neutron star composed of pure nucleonic matter. EOSs computed with the DOPS2 and DOPS3 parameterizations satisfy the X-Ray observational data [Steiner et al., *Astrophys. J.* **722**, 33 (2010)] and the recent observations of GW170817 maximum mass constraint of a stable non-rotating neutron star in the range  $2.01 \pm 0.04 - 2.16 \pm 0.03 M_{\odot}$  [Rezzolla et al., *Astrophys. J. Lett.* **852**, L25 (2018)] and also in good agreement with constraints on mass and radius measurement for PSR J0740+6620 (NICER) [Riley et al., *Astrophys. J. Lett.* **918**, Riley et al., L27 (2021), Miller et al., *Astrophys. J. Lett.* **918**, L28 (2021)]. The hybrid EOSs obtained with the NJL model also satisfy astrophysical constraints on the maximum mass of a neutron star from PSR J1614-2230 [Demorest et al., *Nature* **467**, 1081 (2010)]. We also present the results for dimensionless tidal deformability,  $\Lambda$  which are consistent with the waveform models analysis of GW170817.

## I. INTRODUCTION

The knowledge of neutron star properties is necessary to probe the high density behavior of the equations of state (EOSs) for the baryonic matter in the beta equilibrium. Neutron stars are the densest manifestations of massive objects in the observable universe and sound knowledge of EOSs of dense matter is required to understand the properties of neutron stars. The precise gravitational mass and radius measurements of the neutron stars are effective ways to constrain the EOSs of high dense matter in its interiors. The mass measurement of MSP J0740+6620 [1] with  $2.14^{+0.10}_{-0.09} M_{\odot}$ , is likely to be the most massive neutron star yet observed. Recently, the simultaneous measurements of gravitational mass  $M$  and equatorial circumferential radius  $R_{eq}$  of PSR J0030+0451 from NICER data by Miller et al. [2] and Riley et al. [3] by using independent methods to actual map of the hot region of pulsar, have inferred  $[M = 1.44^{+0.15}_{-0.14} M_{\odot}, R_{eq} = 13.02^{+1.24}_{-1.06} \text{km}]$  and  $[M = 1.34^{+0.15}_{-0.16} M_{\odot}, R_{eq} = 12.71^{+1.14}_{-1.19} \text{km}]$ , respectively.

Theoretically, the investigations of the observed masses and radii of Compact Stars (CS) reveals the particle com-

position and phase transition of dense nuclear matter at high densities. Several attempts [4–7] have been made to construct the EOSs comprising of nucleons, hyperons and quarks under the constraint of global  $\beta$ -equilibrium. The inclusion of hyperons and/or quarks in EOSs softens the high density behavior, leading to the reduction of maximum gravitational masses of CS. Recently, there are many EOS models that include hyperons as well as quark matter [6, 8] and maximum gravitational mass calculated from them is compatible with  $\approx 2M_{\odot}$ .

The theory of strong interactions, quantum chromodynamics (QCD), and ultra-relativistic heavy-ion collisions predict that at high densities, the hadronic matter may undergo a deconfinement phase consisting of quarks and gluons. Therefore, recently, it is an open question whether the inner core of compact stars (CS) consists of quark matter [9–13]. However, this has been suggested currently that the dense nuclear matter in the interior of stable compact stars with maximum gravitational masses  $M \approx 2.0M_{\odot}$  may exhibit evidence for the presence of quark matter cores [7]. Therefore, the hybrid stars phenomenology offers a unique tool to address the challenge of understanding the phase transition in dense quantum chromodynamics. The nuclear theory studies [14–16] are mainly focusing on understanding the dense matter of compact stars (CS). The recent observations with LIGO and Virgo of GW170817 event [17, 18] of Binary Neutron Stars merger and the discovery of CS

\* virenthakur2154@gmail.com

† raj.phy@gmail.com

‡ shashi.dhiman@gmail.com

with masses around  $2M_{\odot}$  [2, 3, 19–22] have intensified the interest in these astonishing objects. The analysis of GW170817 has demonstrated the potential of gravitational wave (GW) observations to yield new information relating to the limits on CS tidal deformability. In addition to these astrophysical observations [5, 23–26], the measurements of rotation frequencies of the pulsar can be employed to constraints the particle composition and behavior of EOSs of the dense nuclear matter. However, the direct measurement of radius and quark matter interior core of CS is still a great challenge from astrophysical interests. In many papers, the properties of cold quark matter have been studied in terms of the phenomenological MIT quark bag model and EOSs at zero temperature have been obtained; these are the basis of calculations of the characteristics of hybrid hadron-quark stars, as well as of strange quark stars [27–31]. The NJL model [32, 33] has recently often been used to describe quark matter; it was originally proposed for explaining the origin of the nucleon mass taking the spontaneous violation of chiral symmetry into account and was later reformulated for the description of quark matter [34, 35]. This model successfully reproduces many features of QCD [36, 37]. Combining different modifications of the NJL quark model with different models for describing hadron matter, several authors have constructed hybrid EOSs of cold matter and used these to study the properties of neutron stars containing quark matter [38–40].

The quark matter phase of EOSs have been treated by employing phenomenological models with some basic features of QCD, such as, the MIT bag models [41–43] with a bag constant and appropriate perturbative QCD corrections and Nambu-Jona-Lasinio with chiral symmetry and its breaking [44], Non-local chiral quark model [45] and constant speed of sound model [46].

The motivation of the present work is to compute a set of EOSs where the hadronic phase has been calculated within the framework of energy density functionals based on the RMF theory [4] and, the quark matter phase of EOS is computed by using three flavor Nambu-Jona-Lasinio (NJL) model with scalar-isovector and vector-isovector couplings. A plausible set of EOSs for hadron-quark matter is employed to study the structural properties of non-rotating neutron stars which satisfies the astrophysical constraints of GW170817, GW190814, PSR J0740+6620, and other available observational data.

The RMF model used in the present work includes all possible self and mixed interaction terms for the  $\sigma$ ,  $\omega$ , and  $\rho$  mesons. The  $\omega$  meson self-coupling term enables one to vary the high density behavior of EOS without affecting the bulk nuclear matter properties at saturation density. Mixed interaction terms involving  $\rho$  mesons allow ones to significantly vary the density dependence of the symmetry energy coefficient which plays a crucial role in determining the cooling mechanism of a neutron star. We used the RMF model with three newly generated parameter sets DOPS1, DOPS2, and DOPS3 to calculate various EOSs composed of nucleons and nucle-

ons with quarks. The generated parameter sets of the model are calibrated by using the available experimental data [47] on the total binding energy and the charge rms radii for a few closed shell nuclei. We also used the value of neutron skin thickness for the  $^{208}\text{Pb}$  nucleus in our calibration procedure. We employ our EOSs to study the structural properties of non-rotating compact stars (CSs).

The manuscript has been organized as, in section II, we described the theoretical framework which is used to construct the various EOSs for pure nucleonic matter and nucleonic with quark matter. RMF model has been employed to describe the nucleonic phase and the quark matter phase has been obtained from the NJL model. The coexisting phase of hybrid EOSs is obtained by using Glendenning construction based on Gibbs conditions of equilibrium. In section III, we present our new parameterizations for RMF model. In section IV, we present our results for finite nuclei and bulk nuclear matter properties at saturation density. In this section, we also discuss the quality of fits to finite nuclei for the newly generated parameterizations. In section V, we present the set of EOSs generated and the results for the various properties of non-rotating neutron stars are also discussed. The summary is presented in section VI.

## II. THEORETICAL FORMALISM

In this section, we discuss the theoretical model employed to calculate various EOSs of dense nuclear matter in different phases. The newly generated parameter sets DOPS1, DOPS2, and DOPS3 of the RMF model have been successfully applied in describing the properties of finite nuclei and bulk nuclear matter at saturation density. These model parameters have been used to construct neutron stars and hybrid CSs. The quark matter phase of the EOS has been calculated by using the NJL model. The final hybrid EOS is comprised of two separate EOSs for each phase of matter, which are combined by utilizing a Glendenning phase transition construction. [48, 49].

### A. Hadronic Equation of State

In the RMF model, the effective Lagrangian density consists of self and mixed interaction terms for  $\sigma$ ,  $\omega$  and  $\rho$  mesons up to the quartic order in addition to the exchange interaction of baryons with  $\sigma$ ,  $\omega$  and  $\rho$  mesons. The  $\sigma$ , the  $\omega$ , and the  $\rho$  mesons are responsible for the ground state properties of the finite nuclei ranging from low mass to heavy mass region in the periodic table. The mixed interactions terms containing the  $\rho$ -meson field enable us to vary the density dependence of the symmetry energy coefficient and neutron skin thickness in heavy nuclei over a wide range without affecting the other properties of the finite nuclei [50, 51]. In particular, the contri-

bution from the self-interaction of  $\omega$ -meson determines the high density behavior of EOS and structure properties of CSs. [4, 52]. The inclusion of self-interaction of  $\rho$ -meson hardly affects the ground state properties of heavy nuclei and compact stars [52]. The effective lagrangian density for the RMF model generally describes the interaction of the baryons via the exchange of  $\sigma$ ,  $\omega$  and  $\rho$  mesons upto the quartic order. The lagrangian density for the RMF model [4, 53] is given by

$$\begin{aligned}
\mathcal{L} = & \sum_B \bar{\Psi}_B [i\gamma^\mu \partial_\mu - (M_B - g_{\sigma B}\sigma) - (g_{\omega B}\gamma^\mu \omega_\mu \\
& + \frac{1}{2}g_{\rho B}\gamma^\mu \tau_{B\cdot}\rho_\mu)] \Psi_B + \frac{1}{2}(\partial_\mu\sigma\partial^\mu\sigma - m_\sigma^2\sigma^2) \\
& - \frac{\bar{\kappa}}{3!}g_{\sigma N}^3\sigma^3 - \frac{\bar{\lambda}}{4!}g_{\sigma N}^4\sigma^4 - \frac{1}{4}\omega_{\mu\nu}\omega^{\mu\nu} + \frac{1}{2}m_\omega^2\omega_\mu\omega^\mu \\
& + \frac{1}{4!}\zeta g_{\omega N}^4(\omega_\mu\omega^\mu)^2 - \frac{1}{4}\rho_{\mu\nu}\rho^{\mu\nu} + \frac{1}{2}m_\rho^2\rho_\mu\rho^\mu \\
& + \frac{1}{4!}\xi g_{\rho N}^4(\rho_\mu\rho^\mu)^2 \\
& + g_{\sigma N}g_{\omega N}^2\sigma\omega_\mu\omega^\mu \left( a_1 + \frac{1}{2}a_2\sigma \right) \\
& + g_{\sigma N}g_{\rho N}^2\sigma\rho_\mu\rho^\mu \left( b_1 + \frac{1}{2}b_2\sigma \right) \\
& + \frac{1}{2}c_1g_{\omega N}^2g_{\rho N}^2\omega_\mu\omega^\mu\rho_\mu\rho^\mu
\end{aligned} \tag{1}$$

The energy density of the uniform matter within the framework of RMF model is given by;

$$\begin{aligned}
\mathcal{E} = & \sum_{j=B,\ell} \frac{1}{\pi^2} \int_0^{k_j} k^2 \sqrt{k^2 + M_j^{*2}} dk \\
& + \sum_B g_{\omega B}\omega\rho_B + \sum_B g_{\rho B}\tau_{3B}\rho_B\rho + \frac{1}{2}m_\sigma^2\sigma^2 \\
& + \frac{\bar{\kappa}}{6}g_{\sigma N}^3\sigma^3 + \frac{\bar{\lambda}}{24}g_{\sigma N}^4\sigma^4 - \frac{\zeta}{24}g_{\omega N}^4\omega^4 \\
& - \frac{\xi}{24}g_{\rho N}^4\rho^4 - \frac{1}{2}m_\omega^2\omega^2 - \frac{1}{2}m_\rho^2\rho^2 \\
& - a_1g_{\sigma N}g_{\omega N}^2\sigma\omega^2 - \frac{1}{2}a_2g_{\sigma N}^2g_{\omega N}^2\sigma^2\omega^2 \\
& - b_1g_{\sigma N}g_{\rho N}^2\sigma\rho^2 - \frac{1}{2}b_2g_{\sigma N}^2g_{\rho N}^2\sigma^2\rho^2 \\
& - \frac{1}{2}c_1g_{\omega N}^2g_{\rho N}^2\omega^2\rho^2.
\end{aligned} \tag{2}$$

The pressure of the uniform matter is given by

$$\begin{aligned}
P = & \sum_{j=B,\ell} \frac{1}{3\pi^2} \int_0^{k_j} \frac{k^4 dk}{\sqrt{k^2 + M_j^{*2}}} - \frac{1}{2}m_\sigma^2\sigma^2 \\
& - \frac{\bar{\kappa}}{6}g_{\sigma N}^3\sigma^3 - \frac{\bar{\lambda}}{24}g_{\sigma N}^4\sigma^4 + \frac{\zeta}{24}g_{\omega N}^4\omega^4 \\
& + \frac{\xi}{24}g_{\rho N}^4\rho^4 + \frac{1}{2}m_\omega^2\omega^2 + \frac{1}{2}m_\rho^2\rho^2 \\
& + a_1g_{\sigma N}g_{\omega N}^2\sigma\omega^2 + \frac{1}{2}a_2g_{\sigma N}^2g_{\omega N}^2\sigma^2\omega^2 \\
& + b_1g_{\sigma N}g_{\rho N}^2\sigma\rho^2 + \frac{1}{2}b_2g_{\sigma N}^2g_{\rho N}^2\sigma^2\rho^2 \\
& + \frac{1}{2}c_1g_{\omega N}^2g_{\rho N}^2\omega^2\rho^2.
\end{aligned} \tag{3}$$

Here, the sum is taken over nucleons and leptons.

The composition of nuclear matter species  $i=n, p, e^-$  and  $\mu^-$  at fixed baryon number density  $\rho_B = \sum_i B_i\rho_i$  is determined in such a way that the charge neutrality condition,

$$\sum_i q_i\rho_i = 0, \tag{4}$$

and the chemical equilibrium conditions

$$\mu_i = B_i\mu_n - q_i\mu_e, \tag{5}$$

are satisfied, where  $B_i$  and  $q_i$  denote baryon number and electric charge of the species  $i$ .

## B. Quark Matter Equation of State

We use the NJL model [54, 55] to calculate the EOS for the quark phase. By introducing the scalar-isovector and vector-isovector couplings, the lagrangian of the three flavour NJL model can be written as

$$\begin{aligned}
\mathcal{L}_{NJL} = & \bar{q}(\not{\partial} - \hat{m})q + \frac{G_S}{2} \sum_{a=0}^8 [(\bar{q}\lambda_a q)^2 + (\bar{q}\gamma_5\lambda_a q)^2] \\
& + \frac{G_V}{2} \sum_{a=0}^8 [(\bar{q}\gamma_\mu\lambda_a q)^2 + (\bar{q}\gamma_5\gamma_\mu\lambda_a q)^2] \\
& - K \det[\bar{q}(1 + \gamma_5)q] + \det[\bar{q}(1 - \gamma_5)q] \\
& + G_{IS} \sum_{a=1}^3 [(\bar{q}\lambda_a q)^2 + (\bar{q}\gamma_5\lambda_a q)^2] \\
& + G_{IV} \sum_{a=1}^3 [(\bar{q}\gamma_\mu\lambda_a q)^2 + (\bar{q}\gamma_5\gamma_\mu\lambda_a q)^2]
\end{aligned} \tag{6}$$

Here  $q$  denotes the quark field with three flavours  $u, d$  and  $s$ , and three colours;  $\hat{m} = \text{diag}(m_u, m_d, m_s)$  is the current quark mass matrix in three flavour space;  $\lambda_a$  are the flavour SU(3) Gell-Mann matrices with  $\lambda_0 =$

$\sqrt{\frac{2}{3}}\mathbf{I}$ ;  $G_S$  and  $G_V$  are the strength of the scalar and vector coupling, respectively; and  $K$  term represents the six-point Kobayashi-Maskawa-t'Hooft (KMT) interaction that breaks the axial  $U(1)_A$  symmetry. Since the Gell-Mann matrices with  $a = 1-3$  are identical to the Pauli matrices in  $u$  and  $d$  space, the last two terms represent the scalar-isovector and vector-isovector coupling breaking the  $SU(3)$  asymmetry while keeping the isospin symmetry, with  $G_{IS}$  and  $G_{IV}$  the corresponding coupling strength. In the present study, we employ the parameters  $m_u = m_d = 3.6$  MeV,  $m_s = 87$  MeV,  $G_S \Lambda^2 = 3.6$ ,  $K \Lambda^5 = 8.9$ , and the cut off value in the momentum integral  $\Lambda = 750$  MeV which is taken from the references [54, 56, 57]. In the present work, we have used vector coupling  $G_V = 0$  in order to describe the astrophysical constraints (Mass/Radius) of MSP 0740+6620, PSR J1614-2230 [1, 7, 19, 91] as hybrid stars. However, the larger value of vector coupling  $G_V$  can stiffen the resulting EOSs and may lead to different neutron star properties [96]. In the NJL model, the quark masses are dynamically generated as solutions of the gap equation, obtained by imposing that the potential be stationary with respect to variations in the quark condensate  $\langle \bar{q}_i q_i \rangle$ , thus finding

$$M_i = m_i - 2G_S \sigma_i + 2K \sigma_j \sigma_k - 2G_{IS} \tau_{3i} (\sigma_u - \sigma_d) \quad (7)$$

where  $\sigma_i = \langle \bar{q}_i q_i \rangle$  stands for the quark condensate with  $(i,j,k)$  being any permutation number of  $(u,d,s)$ , and  $\tau_{3i}$  is the isospin quantum number of quark, i.e.,  $\tau_{3u} = 1$ ,  $\tau_{3d} = -1$  and  $\tau_{3s} = 0$ . As shown in the Eq. (7),  $\sigma_d$  and  $\sigma_s$  contribute to the  $u$  quark mass through the KMT interaction as well as the scalar-isovector coupling, called the flavor mixing [58, 59] in the constituent quark mass. The quark condensate  $\langle \bar{q}_i q_i \rangle$  and the quark number density  $\rho_i$  are given respectively as below

$$\begin{aligned} \langle \bar{q}_i q_i \rangle &= -2N_c \int \frac{d^3p}{(2\pi)^3} \frac{M_i}{E_i} \\ \rho_i &= 2N_c \int_0^\Lambda \frac{d^3p}{(2\pi)^3} \end{aligned} \quad (8)$$

The above Eq.(8) has to be evaluated self-consistently with Eq.(7), forming a set of six coupled equations for the constituent masses  $M_i$ . Once the self-consistent solutions are found, we can calculate the energy density and the pressure in the following form [55],

$$\begin{aligned} \epsilon_{NJL} &= -2N_c \int_0^\Lambda \frac{d^3p}{(2\pi)^3} E_i + G_S (\sigma_u^2 + \sigma_d^2 + \sigma_s^2) \\ &\quad - 4K \sigma_u \sigma_d \sigma_s + G_V (\rho_u^2 + \rho_d^2 + \rho_s^2) \\ &\quad + G_{IS} (\sigma_u - \sigma_d)^2 + G_{IV} (\sigma_u - \sigma_d)^2 - \epsilon_0 \end{aligned} \quad (9)$$

In Eq. (9),  $\epsilon_0$  is introduced to ensure that  $\epsilon_{NJL} = 0$  in the vacuum. The pressure for the cold quark matter can be calculated from the following equation

$$P = \sum_{i=u,d,s} \mu_i \rho_i - \epsilon_{NJL} \quad (10)$$

### C. Coexisting Phase

We construct the EOS of coexisting phase (CP) made up of the hadron phase (HP) and quark matter phase for the hybrid compact star by implementing the Glendenning construction [48, 49]. The evolution of coexisting phase is favored when the surface tension between Coulomb interaction hadronic and quark matter is smaller [60] and negligible. The calculation of surface tension is very model dependent [60, 61]. For the higher values of surface tension, the phase transition is sharp and this is to be constructed with Maxwell construction and in the same way, low values of the phase transition is continuous and that is to be constructed with Glendenning construction. Since the value of surface tension is not established yet, both of the methods of coexisting phase construction are equally valid. But, we adopted the Glendenning construction based on the Gibbs condition of equilibrium. The equilibrium chemical potential of the coexisting phase corresponding to the intersection of the two surfaces representing hadron and quark matter phase can be calculated for mechanical and chemical equilibrium at zero temperature with the following relation,

$$P_{HP}(\mu_e, \mu_n) = P_{NJL}(\mu, \mu_e) = P_{CP}, \quad (11)$$

where  $P_{HP}$ ,  $P_{NJL}$ , and  $P_{CP}$  are the pressures of the hadron phase, quark phase, and coexisting phase, respectively. In coexisting phase, we have considered chemical equilibrium at the hadron-quark interface as well as inside each of the phases [62], so that Eq.(5) implies

$$\mu_u + \mu_e = \mu_d = \mu_s, \quad (12)$$

$$\mu_p + \mu_e = \mu_n = \mu_u + 2\mu_d. \quad (13)$$

In the coexisting phase, the local charge neutrality condition is replaced by the global charge neutrality which means that both hadron and quark matter is allowed to be charged separately. The condition of the global charge neutrality determines the volume fraction  $\chi$  of the quark phase and that can be obtained by using,

$$\chi \rho_c^{NJL} + (1 - \chi) \rho_c^{HP} = 0, \quad (14)$$

where, the  $\rho_c^{NJL}$  and  $\rho_c^{HP}$  are the charge densities of the NJL phase and hadron phase of dense matter, respectively. The value of the  $\chi$  increases from zero in the pure hadron phase to  $\chi = 1$  in the pure quark phase. The energy density  $\mathcal{E}_{CP}$  and the baryon density  $\rho_{CP}$  of the coexisting phase can be calculated as,

$$\mathcal{E}_{CP} = \chi \mathcal{E}_{NJL} + (1 - \chi) \mathcal{E}_{HP}, \quad (15)$$

$$\rho_{CP} = \chi \rho_{NJL} + (1 - \chi) \rho_{HP}. \quad (16)$$

The coexisting phase of EOSs has been computed by employing the procedure explained above and Eqs.(11-15).

### D. Tidal deformability

The tidal influences of its companion in BNS system will deform CS in binary system and, the resulting change in the gravitational potential modifies the BNS orbital motion and its corresponding gravitational wave (GW) signal. This effect on GW phasing can be parameterized by the dimensionless tidal deformability parameter,  $\Lambda_i = \lambda_i/M_i^5$ ,  $i = 1, 2$ . For each CS, its quadrupole moment  $\mathcal{Q}_{j,k}$  must be related to the tidal field  $\mathcal{E}_{j,k}$  caused by its companion as,  $\mathcal{Q}_{j,k} = -\lambda\mathcal{E}_{j,k}$ , where,  $j$  and  $k$  are spatial tensor indices. The dimensionless tidal deformability parameter  $\Lambda$  of a static, spherically symmetric compact star depends on the neutron star compactness parameter  $C$  and a dimensionless quadrupole Love number  $k_2$  as,  $\Lambda = (2k_2/3)C^{-5}$ . The  $\Lambda$  critically parameterizes the deformation of CS under the given tidal field, therefore it should depend on the EOS of nuclear dense matter. When the orbital separation is very small at the frequencies in the BNS systems, the tidal corrections are added to the tidal energy and luminosity linearly to the point-particle energy and luminosity. The leading-order tidal corrections are Newtonian effects and, are known as 5PN (Post Newtonian) and next-to-leading-order 6PN corrections to the energy and luminosity [63, 64]. These leading-order tidal corrections are required to be included in the waveform model employed for analysis of GW signals from advanced LIGO and Virgo GW detectors at the high frequencies, as discussed for the various waveforms by Abbott et al, [18].

To measure the Love number  $k_2$  along with the evaluation of the TOV equations we have to compute  $y_2 = y(R)$  with initial boundary condition  $y(0) = 2$  from the first-order differential equation [65–68] simultaneously,

$$y' = \frac{1}{r}[-r^2Q - ye^\lambda\{1 + 4\pi Gr^2(P - \mathcal{E})\} - y^2], \quad (17)$$

where  $Q \equiv 4\pi Ge^\lambda(5\mathcal{E} + 9P + \frac{\mathcal{E} + P}{c_s^2}) - 6\frac{e^\lambda}{r^2}\nu^2$  and  $e^\lambda \equiv (1 - \frac{2Gm}{r})^{-1}$  and,  $\nu \equiv 2G e^\lambda (\frac{m + 4\pi Pr^3}{r^2})$ . First, we get the solutions of Eq.(17) with boundary condition,  $y_2 = y(R)$ , then the electric tidal Love number  $k_2$  is calculated from the expression as,

$$k_2 = \frac{8}{5}C^5(1 - 2C)^2[2C(y_2 - 1) - y_2 + 2]\{2C(4(y_2 + 1)C^4 + (6y_2 - 4)C^3 + (26 - 22y_2)C^2 + 3(5y_2 - 8)C - 3y_2 + 6) - 3(1 - 2C)^2(2C(y_2 - 1) - y_2 + 2)\log(\frac{1}{1 - 2C})\}^{-1}. \quad (18)$$

### III. NEW RMF MODEL PARAMETERIZATION

There are several relativistic mean field models in which energy density functional consists of nonlinear  $\sigma$ ,  $\omega$  and  $\rho$  terms and mixed interaction terms. These models are used to construct the EOSs composed of nucle-

onic matter [69] and nucleonic along with hyperonic matter [70, 71] and accosted with the constraints of nuclear matter properties and astrophysical observations of CS masses [3, 20, 22]. Only RMF models BSR [4] with  $\zeta = 0$  and NL3 $\omega\delta$  [72] can sustain the condition of maximum mass  $M \geq 2.0M_\odot$  when hyperons are included in the EOSs with appropriate meson-hyperon couplings, otherwise, the inclusion of hyperons may lead for the famous hyperon puzzle. However, many RMF models [73] without the inclusion of hyperons satisfy the constraints of astrophysical observations obtained from binary neutron star merger event GW170817. In the present work, we search for the best fit parameters of RMF model by using simulated annealing method to minimise the  $\chi^2$  [74, 75] which is given by

$$\chi^2 = \frac{1}{N_d - N_p} \sum_{i=1}^{N_d} \left( \frac{M_i^{exp} - M_i^{th}}{\delta_i} \right)^2 \quad (19)$$

where,  $N_d$  is the number of experimental data points and  $N_p$  the number of fitted parameters. The  $\delta_i$  stands for theoretical error [97] and  $M_i^{exp}$  and  $M_i^{th}$  are the experimental and the corresponding theoretical values, respectively, for a given observable. Since  $M_i^{th}$  in Eq. (19) are calculated by using RMF model, the value of  $\chi^2$  depends on the parameters appearing in Eq. (1). The theoretical errors  $\delta_i$  in Eq. (19) are taken to be 1.0 MeV for total binding energies, 0.02 fm for the charge rms radii and 0.005 fm for the neutron skin thickness. Three new parameter sets namely DOPS1, DOPS2, and DOPS3 have been generated by including all possible self and mixed interaction terms for  $\sigma$ ,  $\omega$  and  $\rho$  mesons up to quartic order for a fixed value of  $\omega$  meson self-coupling parameter  $\zeta = 0.00, 0.01$  and  $0.02$ . The remaining coupling parameters are determined by fitting the RMF results to the available experimental data for total binding energies for  $^{16,24}\text{O}$ ,  $^{40,48}\text{Ca}$ ,  $^{56,78}\text{Ni}$ ,  $^{88}\text{Sr}$ ,  $^{90}\text{Zr}$ ,  $^{100,116,132}\text{Sn}$ , and  $^{208}\text{Pb}$  nuclei and charge rms radii for  $^{16}\text{O}$ ,  $^{40,48}\text{Ca}$ ,  $^{56}\text{Ni}$ ,  $^{88}\text{Sr}$ ,  $^{90}\text{Zr}$ ,  $^{116}\text{Sn}$ , and  $^{208}\text{Pb}$  nuclei as per the available experimental data [47]. In addition, we also fit the value of neutron skin thickness for the  $^{208}\text{Pb}$  nucleus which is a very important physical observable. Recently extracted values of neutron skin thickness for the  $^{208}\text{Pb}$  nucleus from isospin diffusion data lie within  $0.16 - 0.33\text{fm}$  indicating large uncertainties [76, 77, 98]. It is also shown in ref. [99] that neutron skin thickness of  $\approx 0.18\text{fm}$  in the  $^{208}\text{Pb}$  nucleus is required to adequately reproduce the centroid energies of isoscalar giant monopole and isovector giant dipole resonances. We include in our fit, the value of neutron skin thickness  $\Delta r = 0.18\text{fm}$  for the  $^{208}\text{Pb}$  nucleus to constrain the linear density dependence of the symmetry energy coefficient. The DOPSs parameter sets have been generated for a fixed value of  $\omega$ -meson self-coupling parameter  $\zeta = 0.00, 0.01$ , and  $0.02$  in the light of the recent observation of GW190814, GW170817, and PSR J0740+6620. The coupling parameter  $\zeta$  affects the high density behavior of the EOS. A large value of  $\zeta$  makes the EOS softer and a smaller value stiffens the

EOS. The value of maximum mass for GW190814 event lies in the range  $2.50$ - $2.67 M_{\odot}$  [90], which requires stiff EOS and hence a very small value of  $\zeta$  which we have taken equal to zero for DOPS1 parameterization. The astrophysical events GW170817 and PSR J0740+6620 have maximum mass  $\approx 2 M_{\odot}$  and require relatively softer EOSs. For this, we have fixed the value of  $\zeta$  equal to  $0.01$  and  $0.02$  for DOPS2 and DOPS3 parameter sets respectively. The  $\rho$  meson self interaction has not been included as it hardly affects the properties of finite nuclei and neutron star [52].

In Table I, the newly generated parameter sets DOPS1, DOPS2 and DOPS3 are listed. We also display the value of parameters for NL3 [78], FSUGarnet [79], IOPB-1 [80] and Big Apple [77]. The effective field theory imposes the condition of naturalness [81] on the parameters or expansion coefficients appearing in the energy density functional Eq. (2). According to naturalness, the coefficients of various terms in energy density functional should be of same size when expressed in appropriate dimensionless ratio. The dimensionless ratios are obtained by dividing Eq. (2) by  $M^4$  and expressing each term in powers of  $\frac{g_{\sigma}\sigma}{M}$ ,  $\frac{g_{\omega}\omega}{M}$  and  $2\frac{g_{\rho}\rho}{M}$ . This means that the dimensionless ratios  $\frac{1}{2C_{\sigma}^2 M^2}$ ,  $\frac{1}{2C_{\omega}^2 M^2}$ ,  $\frac{1}{8C_{\rho}^2 M^2}$ ,  $\frac{\bar{\kappa}}{6M}$ ,  $\frac{\bar{\lambda}}{24M}$ ,  $\frac{\zeta}{24}$ ,  $\frac{a_1}{M}$ ,  $\frac{a_2}{2}$ ,  $\frac{b_1}{4M}$ ,  $\frac{b_2}{8}$  and  $\frac{c_1}{8}$  should be roughly of same size, where  $c_i^2 = \frac{g_i^2}{m_i^2}$ ,  $i$  denotes  $\sigma$ ,  $\omega$  and  $\rho$  mesons. In Table II, we present the overall naturalness behavior of various parameterizations i.e. the value of these parameters when expressed in dimensionless ratios as shown just above. We also display the corresponding values for NL3, FSUGarnet, IOPB-1, and Big Apple parameter sets. It is clear from the table that the DOPS1, DOPS2, and DOPS3 parameterizations closely favor the naturalness behavior. It can also be seen from table II, that the value of parameter  $c_1$  (mixed interaction term of  $\omega^2\rho^2$ ) is very large and equal to  $10.75$ ,  $6.0$  and  $11.75$  for FSUGarnet, IOPB-1 and Big Apple parameterizations respectively when expressed in appropriate dimensionless ratio. The large value of  $c_1$  gives rise to the deviation from the naturalness behavior and this deviation might be attributed to the fact of not including all possible mixed interaction terms of  $\sigma$ ,  $\omega$  and  $\rho$  mesons in these respective parameterizations, unlike DOPSs parameterizations. As far as NL3 parameterization is concerned, the naturalness behavior is favored very well but it does not include any cross interaction terms of sigma, omega, and rho mesons which are very important for constraining the symmetry energy and its density dependence. DOPS1, DOPS2, and DOPS3 parameterizations show better naturalness behavior as compared to other parameterizations displayed in the table. The naturalness behavior of parameters can be further improved by considering the next higher order terms containing the gradient of fields [81].

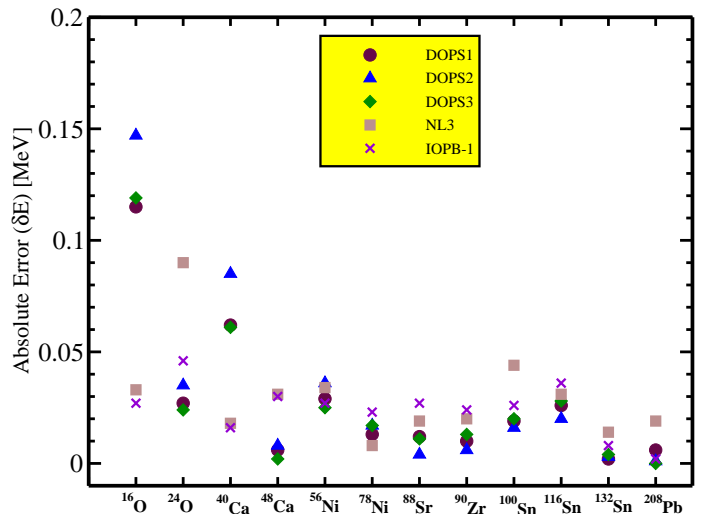


FIG. 1. (Color online) Absolute error in the binding energy per nucleon ( $\delta E$ ) plotted against the mass number ( $A$ ) for newly generated parameter sets DOPS1, DOPS2 and DOPS3. For comparison, the values of  $\delta E$  obtained with parameters NL3 and IOPB-1 are also displayed.

#### IV. FINITE NUCLEI AND INFINITE NUCLEAR MATTER

In this section, we discuss our results for finite nuclei and infinite nuclear matter. The newly generated parameterizations DOPS1, DOPS2 and DOPS3 give equally good fit to the properties of finite nuclei. In Fig. (1), we display the value of absolute error in binding energy per nucleon which is defined as,

$$\delta E = |BE^{exp} - BE^{th}| \quad (20)$$

Here,  $BE^{exp}$  and  $BE^{th}$  are the experimental and theoretical values for the binding energy per nucleon respectively. Results for  $\delta E$  are calculated for DOPSs parameterizations. The mean absolute errors in the binding energy per nucleon calculated with the DOPS1, DOPS2, and DOPS3 parameterizations for the finite nuclei used in the fit are  $0.027$ ,  $0.031$ , and  $0.027$  MeV respectively. We also display similar results for NL3, IOPB-1 parameter sets. It is evident that binding energies obtained using DOPSs parameterizations are in good agreement with the available experimental data [47]. In Fig. (2), we present our results for absolute error  $\delta R_{ch} = |R_{ch}^{exp} - R_{ch}^{th}|$  for charge rms radii and also compare them with NL3 and IOPB-1 parameter sets. The value of charge rms radii calculated for various parameterizations displayed in Fig. (2) are more or less same. The mean absolute error in the charge rms radii for DOPS1, DOPS2 and DOPS3 parameterizations for the finite nuclei used in the fit are  $0.019$ ,  $0.022$  and  $0.023$  fm respectively.

We have also calculated the rms errors in the total binding energy and charge radii for the nuclei considered in our fit. The root mean square (rms) errors in total binding energy for all the nuclei considered in our fit are found

TABLE I. Newly generated parameter sets DOPS1, DOPS2 and DOPS3 for the Lagrangian of RMF model as given in Eq.(1). The parameters  $\bar{\kappa}$ ,  $a_1$ , and  $b_1$  are in  $\text{fm}^{-1}$ . The masses  $m_\sigma$ ,  $m_\omega$  and  $m_\rho$  are in MeV. The mass for nucleon is taken as  $M_N = 939\text{MeV}$ . The values of  $\bar{\kappa}$ ,  $\bar{\lambda}$ ,  $a_1$ ,  $a_2$ ,  $b_1$ ,  $b_2$ , and  $c_1$  are multiplied by  $10^2$ . The parameter sets NL3, FSUGarnet, IOPB-1 and Big Apple are also presented.

Parameters	DOPS1	DOPS2	DOPS3	NL3	FSUGarnet	IOPB-1	Big Apple
$g_\sigma$	10.20651	10.67981	10.51853	10.21743	10.50315	10.41851	9.67810
$g_\omega$	12.87969	14.12312	13.53456	12.86762	13.69695	13.38412	12.33541
$g_\rho$	14.13399	14.89809	14.64808	8.94880	13.87880	11.11560	14.14256
$\bar{\kappa}$	2.62033	3.00823	1.97233	1.95734	1.65229	1.85581	2.61776
$\bar{\lambda}$	-1.67616	-0.07894	-0.11438	-1.59137	-0.35330	-0.75516	-2.16586
$\zeta$	0.00000	0.01000	0.02000	0.00000	0.23486	0.017442	0.000699
$\mathbf{a}_1$	0.02169	0.08832	0.01911	0.00000	0.00000	0.00000	0.00000
$\mathbf{a}_2$	0.01785	0.04637	0.02699	0.00000	0.00000	0.00000	0.00000
$\mathbf{b}_1$	0.73554	0.79273	0.77259	0.00000	0.00000	0.00000	0.00000
$\mathbf{b}_2$	0.98545	0.98986	0.89590	0.00000	0.00000	0.00000	0.00000
$\mathbf{c}_1$	0.86916	0.63710	0.70353	0.00000	8.60000	4.80000	9.40000
$m_\sigma$	503.61992	492.84789	502.37396	508.19400	496.93900	500.48700	492.73000
$m_\omega$	782.50000	782.50000	782.50000	782.50100	782.50000	782.18700	782.50000
$m_\rho$	770.00000	770.00000	770.00000	763.00000	763.00000	762.46800	763.00000

TABLE II. The values of parameters expressed as dimensionless ratios corresponding to naturalness behavior. All values have been multiplied by  $10^3$ .

Parameters	DOPS1	DOPS2	DOPS3	NL3	FSUGarnet	IOPB-1	Big Apple
$\frac{1}{2C_\sigma^2 M^2}$	1.3806	1.2076	1.2935	1.4028	1.2690	1.3086	1.4698
$\frac{1}{2C_\omega^2 M^2}$	2.0931	1.7407	1.8959	2.0970	1.8508	1.9383	2.2819
$\frac{1}{8C_\rho^2 M^2}$	0.4207	0.3787	0.3917	1.0306	0.4278	0.6670	0.4121
$\frac{\bar{\kappa}}{6M}$	0.9177	1.0536	0.6908	0.6855	0.5787	0.6499	0.9168
$\frac{\bar{\lambda}}{24M}$	-0.6984	-0.0329	-0.0476	-0.6630	-0.1472	-0.3146	-0.9024
$\frac{\zeta}{24}$	-	0.4166	0.8333	-	0.9785	0.7267	0.0291
$\frac{\mathbf{a}_1}{M}$	0.2169	0.8832	0.1911	-	-	-	-
$\frac{\mathbf{a}_2}{2}$	0.0893	0.2318	0.1349	-	-	-	-
$\frac{\mathbf{b}_1}{4M}$	1.8388	1.9818	1.9315	-	-	-	-
$\frac{\mathbf{b}_2}{8}$	1.2318	1.2373	1.1198	-	-	-	-
$\frac{\mathbf{c}_1}{8}$	1.0864	0.7964	0.8794	-	10.7500	6.0000	11.7500

to be 1.58, 1.63, 1.61, 2.41, and 1.93 MeV for DOPS1, DOPS2, DOPS3, NL3, and IOPB-1 parameterizations respectively. Similarly, the root mean square (rms) errors in charge radii for all nuclei taken in our fit are 0.020, 0.023, 0.024, 0.020, and 0.022 fm for DOPS1, DOPS2, DOPS3, NL3, and IOPB-1 parameter sets respectively. In Table III, we present our results for the symmetric nuclear matter (SNM) properties such as binding energy per nucleon (E/A), incompressibility (K), symmetry energy coefficient (J), density dependence of symmetry energy (L) and the ratio of effective mass to the mass of nucleon

( $M^*/M$ ) at the saturation density ( $\rho_0$ ). These properties are very important for constructing the EOS for nuclear matter. The value of E/A is  $\approx -16$  MeV for all DOPSs parameterizations. For all newly generated parameterizations, the value of J and L are consistent with the constraints from observational analysis  $J = 31.6 \pm 2.66$  MeV and  $L = 58.9 \pm 16$  MeV [82]. The value of K lies in the range 227.5 - 232.733 MeV which is in agreement with the value of  $K = 240 \pm 20$  MeV determined from isoscalar giant monopole resonance (ISGMR) for  $^{90}\text{Zr}$  and  $^{208}\text{Pb}$  nuclei [83, 84]. The ratio of effective mass to

TABLE III. The SNM properties at saturation density for the parameter sets DOPS1, DOPS2 and DOPS3 are compared with that obtained using NL3, FSUGarnet, IOPB-1 and Big Apple parameter sets.  $\rho_0$ ,  $E/A$ ,  $K$ ,  $J$ ,  $L$  and  $M^*/M$  denotes the saturation density, Binding Energy per nucleon, Nuclear Matter incompressibility coefficient, Symmetry Energy coefficient, density dependence of symmetry energy and ratio of effective nucleon mass to the nucleon mass respectively.

Parameters	DOPS1	DOPS2	DOPS3	NL3	FSUGarnet	IOPB-1	Big Apple
$\rho_0$ ( $\text{fm}^{-3}$ )	0.150	0.148	0.148	0.148	0.153	0.149	0.155
$E/A$ (MeV)	-16.073	-16.073	-16.037	-16.248	-16.229	-16.099	-16.339
$K$ (MeV)	231.204	232.733	227.500	271.565	229.623	222.571	227.093
$J$ (MeV)	31.894	31.767	31.843	37.400	30.983	33.303	31.410
$L$ (MeV)	65.590	66.018	66.743	118.563	50.925	63.850	40.339
$M^*/M$	0.604	0.611	0.605	0.595	0.578	0.595	0.608

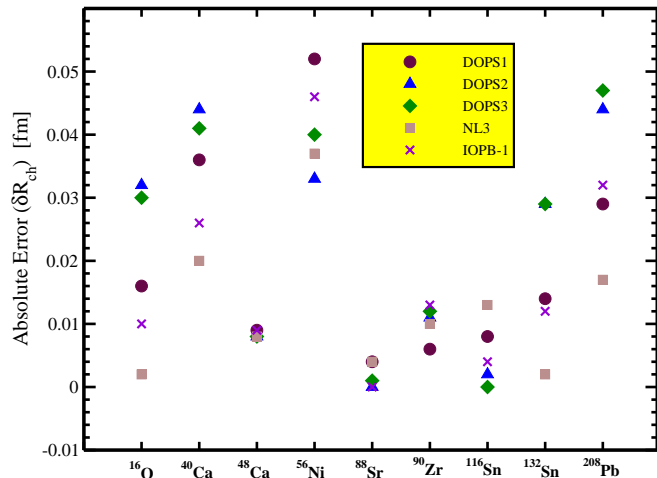


FIG. 2. (Color online) Absolute error in the charge root mean square radii ( $\delta R_{ch}$ ) plotted against the mass number ( $A$ ) for newly generated parameter sets DOPS1, DOPS2 and DOPS3. For comparison, the values obtained with parameters NL3 and IOPB-1 are also displayed.

the nucleon mass is found to be similar for all DOPS parameterizations as shown in Table III. The SNM properties calculated with NL3, FSUGarnet, IOPB-1, and Big Apple are also shown for comparison. In Fig. (3 and 4), we plot the EOS i.e. pressure as a function of baryon density ( $\frac{\rho}{\rho_0}$ ) for SNM and pure neutron matter (PNM) using DOPS1, DOPS2 and DOPS3 parameterizations which is in good agreement and lie in the allowed region with the EOS extracted from the analysis of particle flow in heavy-ion collision [85]. These results are also compared with the NL3 and IOPB-1 parameterizations. It can be easily seen that the EOSs for SNM and PNM obtained from DOPS1 and NL3 parameterizations are very stiff and are ruled out by heavy ion collision data. The stiffness of the EOSs for DOPS1 and NL3 parameter sets may be due to the fact that the coupling parameter  $\zeta$  which varies the high density behavior of EOS is taken to be equal to zero. The stiff EOS obtained by DOPS1 is

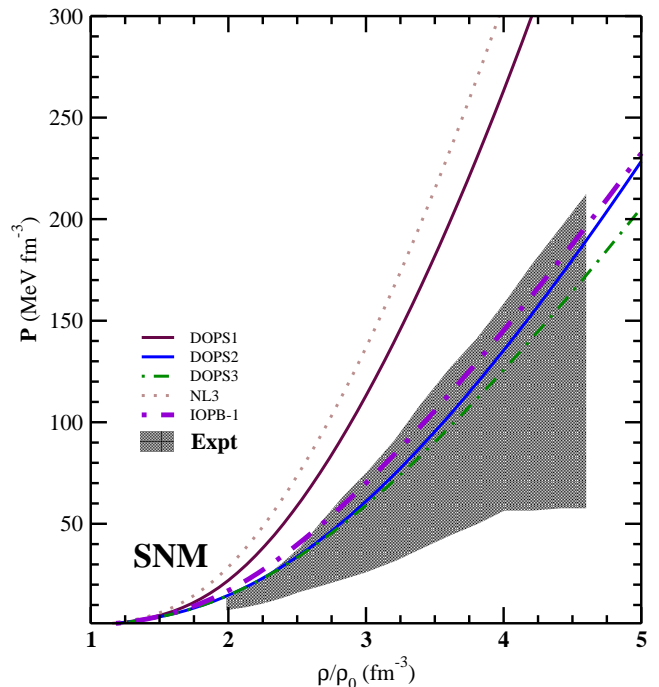


FIG. 3. (Color online) Variation of Pressure as a function of baryon density for symmetric nuclear matter (SNM) computed with DOPS1, DOPS2 and DOPS3 parameterizations along with NL3 and IOPB-1. The shaded region represents the experimental data taken from the reference [85].

required to account for the predicted supermassive neutron star in GW190814 event. The EOSs calculated using DOPS2 and DOPS3 parameter sets are much softer and lie in the allowed region of heavy ion collision data [85]. The softness of EOSs is attributed to the large value of  $\zeta$ .

DOPS1 gives Stiffest EOS among DOPS parameter sets and hence a large value of energy density and pressure at a given baryon density. The parameter sets DOPS2 and DOPS3 give relatively softer EOSs and comparatively smaller value of pressure and energy density. Due to this



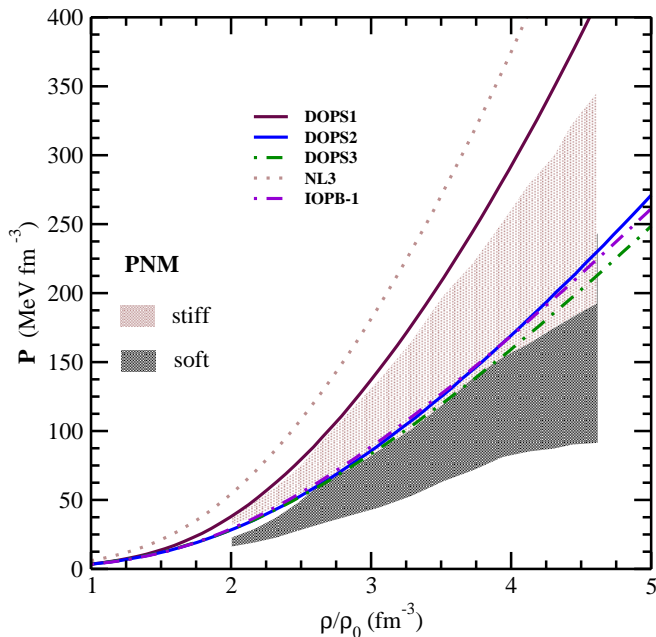


FIG. 4. (Color online) Variation of Pressure as a function of baryon density for pure neutron matter (PNM) computed with DOPS1, DOPS2 and DOPS3 parameterizations along with NL3 and IOPB-1. The shaded region represents the experimental data taken from the reference [85].

fact, the lines for model DOPS1 are so much different than that of DOPS2 and DOPS3 model parameterization as shown in Fig. (3 and 4).

## V. EQUATION OF STATE AND NEUTRON STAR PROPERTIES

Here we discuss the results for the properties of non-rotating neutron stars for a set of EOSs obtained using different parameterizations in the hadronic phase, uds quark phase, and coexisting phase. We employed the Baym-Pethick-Sutherland (BPS) [86] EOS for low density regime from outer crust baryon density ( $\rho = 6.3 \times 10^{-12}$ ) up to the pasta phase ( $\rho = 9.4 \times 10^{-2}$ ). The crust region and the core region of the EOSs have been matched by using the cubic interpolation method that offers true continuity between the crust and the core.

In Table IV, we list the various EOSs, their particle compositions and properties of non-rotating neutron stars like maximum gravitational mass ( $M_G$ ), radius  $R_{max}$ , ( $R_{1.4}$ ) and dimensionless tidal deformability  $\Lambda_{1.4}$  of canonical mass. The properties like mass and radius for the neutron star are calculated by integrating the Tolman-Oppenheimer-Volkoff (TOV) equations [87]. TOV equations are solved for various EOSs consisting of nucleonic and nucleonic with quark matter. The composition at any density is so determined that the charge neutrality and beta equilibrium conditions hold good. A set of EOSs used in the present work has been dis-

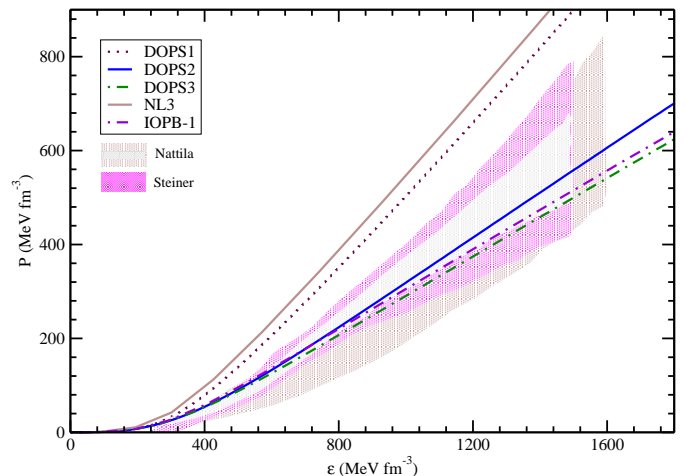


FIG. 5. (Color online) Variation of pressure with energy density for EOSs calculated with DOPS1, DOPS2, DOPS3, NL3 and IOPB-1 parameterizations. The shaded region (magenta) represents the observational constraints from Ref. [88] and the regions (orange and cyan) denote the EOS of cold dense matter with 95 % confidence limit [89].

played in Table IV where DOPS1, DOPS2, and DOPS3 are pure hadronic (nucleonic) EOSs computed with the newly generated DOPSs parameterizations. The EOSs namely DOPS1Q, DOPS2Q, and DOPS3Q composed of nucleons and quarks in beta equilibrium with the NJL coexisting phase are also presented. For the sake of comparison, the results for EOSs calculated with NL3, FSUGarnet, IOPB-1 and Big Apple parameters are also presented. In Fig. (5), we display the variation of pressure with energy density for various EOSs composed of pure nucleonic matter. The results are also compared with NL3 and IOPB-1 parameter sets. The shaded region (magenta color) represents the observational constraints from the ref. [88] and regions (brown and grey) denote the EOS of cold dense matter with 95 % confidence limit [89]. It is clear that EOS computed with DOPS1 parameter set is very stiff like NL3 and is required to account for supermassive neutron star as predicted by GW190814 event and is ruled out by the above observational constraints. The EOSs calculated with DOPS2, DOPS3, and IOPB-1 are relatively softer and are in well agreement with the observational constraints as shown in Fig. (5).

In Fig. (6), we plot the results for hybrid EOSs composed of nucleons and quark matter with a coexisting phase in  $\beta$ -equilibrium. The nucleonic part of the EOS is calculated by using DOPSs parameterizations and the pure quark phase is described with three flavor NJL model as discussed in Section II. For the coexisting phase of hadronic matter and quark matter, the Glendenning construction method has been employed along with the global charge neutrality condition. The solid circles represent the boundary of coexisting phase region which consists of nucleons and quarks. The coexisting phase

TABLE IV. The properties of non-rotating compact stars for the various EOSs along with their particle composition computed with the newly generated parameter sets are presented. Results are also displayed for other parameter sets.  $M_G(M_\odot)$  and  $R_{max}$  denote the Maximum Gravitational mass and radius corresponding to the maximum mass of the non-rotating compact stars respectively. The values for  $R_{1.4}$  and  $\Lambda_{1.4}$  denote radius and dimensionless tidal deformability at  $1.4M_\odot$ .

No.	EOS	Particle composition	$M(M_\odot)$	$R_{max}$ (km)	$R_{1.4}$ (km)	$\Lambda_{1.4}$
1	DOPS1	n,p,e, $\mu$	2.57	12.36	13.61	627.37
2	DOPS2	n,p,e, $\mu$	2.12	11.56	13.24	546
3	DOPS3	n,p,e, $\mu$	2.05	11.61	13.25	563.2
4	DOPS1Q	n,p,e, $\mu$ ,u,d,s	2.23	13.22	13.60	637
5	DOPS2Q	n,p,e, $\mu$ ,u,d,s	1.95	12.39	13.25	527.3
6	DOPS3Q	n,p,e, $\mu$ ,u,d,s	1.91	12.35	13.26	547.2
7	NL3	n,p,e, $\mu$	2.73	13.10	14.65	1234.8
8	FSUGarnet	n,p,e, $\mu$	2.06	11.70	12.86	624.8
9	IOPB-1	n,p,e, $\mu$	2.16	12.22	14.09	833
10	Big Apple	n,p,e, $\mu$	2.6	12.41	12.96	717.3

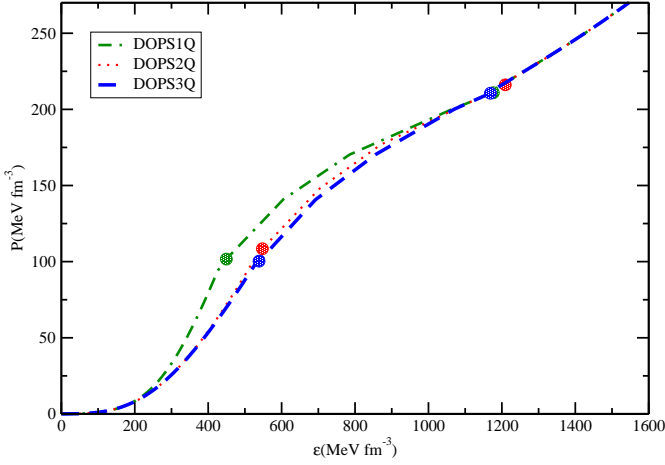


FIG. 6. (Color online) Variation of pressure with energy density for hybrid EOSs DOPS1Q, DOPS2Q and DOPS3Q composed of pure nucleonic matter, quark matter and NJL coexisting phase. The solid circles represent the boundary of coexisting phase comprised of nucleons and quarks.

region lies in the density ranging from  $2.88\rho_0 - 6.5\rho_0$ ,  $3.49\rho_0 - 6.71\rho_0$  and  $3.43\rho_0 - 6.57\rho_0$  for DOPS1, DOPS2 and DOPS3 respectively. The coexisting phase region for the DOPS1 region is large as compared to others. As DOPS1 parameter set produces a stiff EOS and thus the coexisting phase region lies in the higher pressure region.

In Fig. (7), we plot the gravitational mass ( $M_G$ ) of the neutron star as a function of the baryon density for various EOSs considered in the present work. It is evident from the figure that gravitational mass increases with the increase in baryon density to obtain its maximum value. It is quite obvious that the maximum gravitational mass is corresponding to the stiffest EOS and goes on decreasing as the EOS becomes softer. In Fig. (8), we have also shown the proton fraction as a function of baryon density for various EOSs.

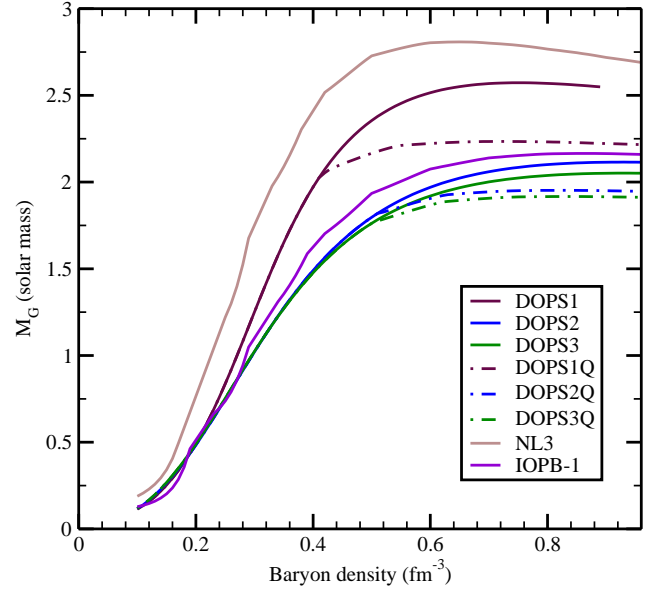


FIG. 7. (Color online) Gravitational mass ( $M_G$ ) for the non-rotating compact stars as a function of baryon density for various EOSs.

Fig. (9), presents our results for the gravitational mass of non-rotating neutron star and its radius for DOPSS parameterizations. The results are also displayed for NL3 and IOPB-1 parameter sets. The maximum mass of non-rotating neutron star obtained for EOS calculated with the DOPS1 parameter set is found to be  $2.57M_\odot$  with a radius of 12.36 Km. This maximum mass obtained with the DOPS1 parameter satisfies the constraint from GW190814 event which gives the mass range between  $2.50 - 2.67 M_\odot$  [90] indicating that the secondary component might be the heaviest neutron star composed of nucleonic matter. This parameter set also satisfies the recently measured radius of PSR J0740+6620 with

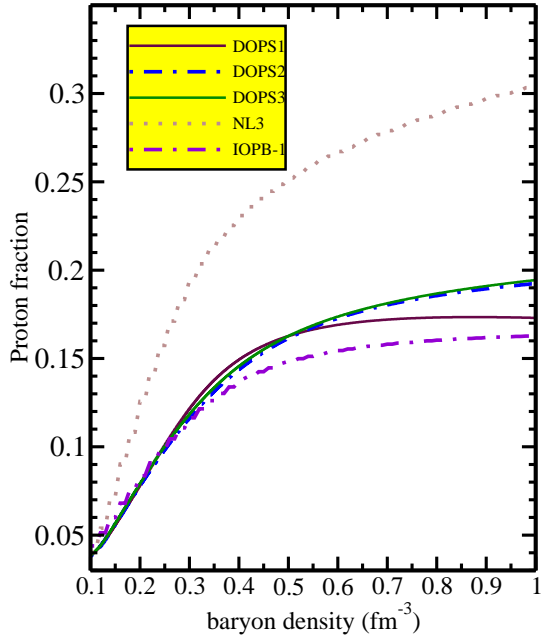


FIG. 8. (Color online) Proton fraction plotted against the baryon density.

$= 12.39^{+1.30}_{-0.98}$  Km radius by NICER [91]. DOPS2 and DOPS3 sets produce non-rotating neutron stars of maximum mass  $2.05M_{\odot}$  and  $2.12M_{\odot}$  with the radius of 11.56 Km and 11.61 Km respectively. The radii of canonical mass  $R_{1.4}$  for DOPS2 and DOPS3 are calculated to be 13.24 Km and 13.25 Km respectively. The DOPS2 and DOPS3 parameter sets satisfy the mass constraints from GW170817 [92], PSR 0740+6620, NICER [91, 93] and radius constraints from NICER [2, 3, 7, 91] and is also very close to the upper limit of the radius constraint [93]. The hybrid EOSs namely DOPS1Q, DOPS2Q, and DOPS3Q produce the hybrid star with a maximum mass of 2.23, 1.95, and 1.91  $M_{\odot}$  respectively. The phase transition from hadron to quark matter lowers the maximum mass as EOS becomes softer and, accordingly the maximum mass reduces from 2.57 to 2.23  $M_{\odot}$ , 2.12 to 1.95  $M_{\odot}$  and 2.05 to 1.91  $M_{\odot}$  corresponding to DOPS1, DOPS2, and DOPS3 parameterizations respectively. The reduction in the maximum mass is found to be more in the stiffest EOS i.e. DOPS1. The hybrid EOS DOPS1Q satisfies the mass constraint of MSP 0740+6620 [1]. The DOPS2Q and DOPS3Q EOSs satisfy the mass constraint from PSR J1614-2230 [19]. These hybrid EOSs satisfy the radius constraint from NICER [7, 91]. The various observational constraints on maximum mass and radius measurements from recently observed astrophysical events PSR J0740+6620 [91, 93], PSR J1614+2230 [19], PSR J0348+432 [20] and GW190814 [90] are also shown in Fig. (9). Similar results for NL3 and IOPB-1 parameter sets are also displayed.

The dimensionless tidal deformability ( $\Lambda_{1.4}$ ) obtained by employing EOSs namely DOPS2, DOPS3, DOPS2Q and

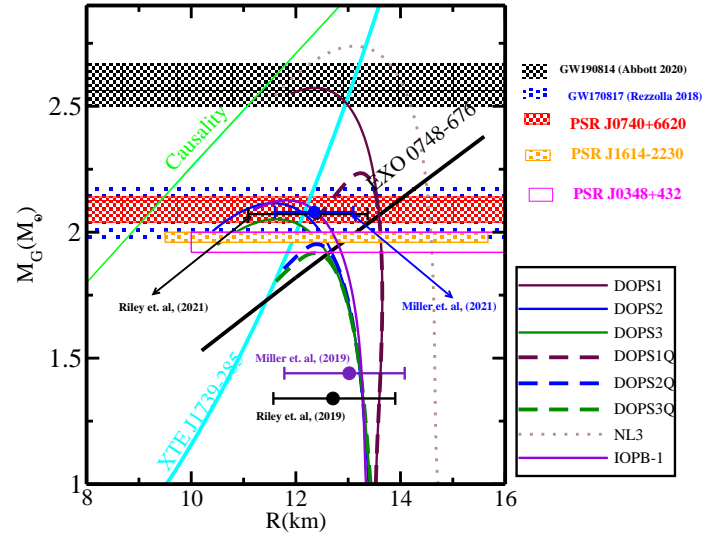


FIG. 9. (Color online) Mass-Radius profile for pure nucleonic and hybrid non-rotating neutron star for various EOSs. The recently observed constraints on mass and radius measurements from recently observed astrophysical events PSR J0740+6620 [2, 3, 91, 93], PSR J1614+2230 [19], PSR J0348+432 [20], GW190814 [90] and GW170817 [92] are also depicted. The region excluded by causality (solid green line), rotation constraint of neutron star XTE J1739-285 (solid cyan line) and limits on Mass-Radius of compact star from Özel’s analysis of EXO 0748-676 are also shown.

DOPS3Q considered in the present work lie in the range 527 - 563 as one can see in Table IV. These values satisfy the constraint on  $\Lambda_{1.4} = 190^{+390}_{-120}$  [17, 94]. The dimensionless tidal deformability ( $\Lambda_{1.4}$ ) for EOSs DOPS1 and DOPS1Q are 627 and 637 respectively and is consistent with the constraints on dimensionless tidal deformability obtained using Bayesian analysis  $\Lambda_{1.4} = 500^{+186}_{-367}$  [95].

In Fig. (10), we plotted  $\Lambda$  as a function of gravitational mass. It is obvious from the Fig. (10) that  $\Lambda$  decreases with the increase in gravitational mass of compact stars and reduces to very small value at the maximum mass. The recent observational limits on  $\Lambda_{1.4}$  [17, 95] are also displayed in Fig. (10).

## VI. SUMMARY

Theoretical studies of dense matter have considerable uncertainty in the high density behavior of the EOSs largely because of the poorly constrained many-body interactions. The theoretical study of the structure of neutron stars is crucial if new observations of masses and radii lead to effective constraints on the EOSs of dense matter. GW170817, GW190814, and PSR J0740 + 6620 etc. are some of those recent astrophysical observations (constraints) to which our study is devoted. This study can further prompt the theoretical/experimental(astrophysical observations) investiga-

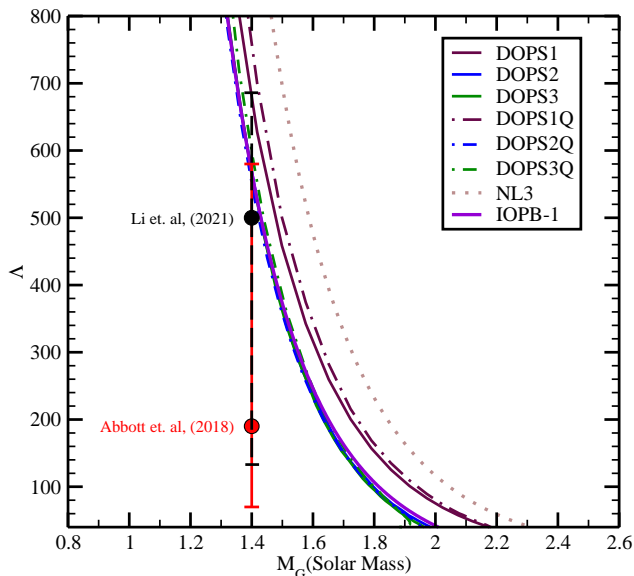


FIG. 10. (Color online) Variation of dimensionless tidal deformability ( $\Lambda$ ) with respect to gravitational mass of non-rotating compact stars for various EOSs. The recent constraints on  $\Lambda_{1.4}$  from Ref. [17, 95] are also depicted

tions. The present study demonstrates that the contributions of self and mixed interactions of  $\sigma$ ,  $\omega$ , and  $\rho$  mesons up to quartic order are important to vary the high density behavior of EOS and favor the naturalness behavior of parameters.

We have studied the properties of finite nuclei, infinite nuclear matter, and compact stars with newly generated parameter sets DOPS1, DOPS2, and DOPS3 of field theoretical relativistic mean field (RMF) models which include all the possible self and mixed interactions between the scalar-isoscalar ( $\sigma$ ), vector-isoscalar ( $\omega$ ) and vector-isovector ( $\rho$ ) mesons up to quartic order. The generated parameter sets are in harmony with the finite and bulk nuclear matter properties. All these generated parameterizations fit equally well the finite nuclear properties and closely favor the naturalness behavior [81]. The mean absolute errors in the binding energy per nucleon calculated with the DOPS1, DOPS2, and DOPS3 parameterizations for the finite nuclei used

in the fit are 0.027, 0.031, and 0.027 MeV respectively. Similarly, the mean absolute error in the charge rms radii for DOPS1, DOPS2, and DOPS3 parameterizations for the finite nuclei used in the fit are 0.019, 0.022 and 0.023 fm respectively. The maximum mass of a non-rotating star with DOPS1 parameterization is found to be around  $2.6 M_{\odot}$  for the pure hadronic matter which satisfies the recent GW190814 possible maximum mass constraint [90] indicating that the secondary component of GW190814 could be the non-rotating neutron star consisting of pure nucleonic matter. This parameter set also satisfies the recently measured constraints on the radius for PSR J0740+6620 with  $12.39^{+1.30}_{-0.98}$  Km by NICER [91]. DOPS2 and DOPS3 sets produce non-rotating neutron stars of maximum mass  $2.05 M_{\odot}$  and  $2.12 M_{\odot}$  with the radius of 11.56 Km and 11.61 Km respectively. The radius of canonical mass  $R_{1.4}$  for DOPS2 and DOPS3 are calculated to be 13.24 Km and 13.25 Km respectively. The DOPS2 and DOPS3 parameter sets satisfy the mass constraints of PSR 0740+6620, NICER [91, 93] and radius constraints from NICER [2, 3, 7, 91] and is also very close the upper limit of the radius constraint [93]. EOSs computed with the DOPS2 and DOPS3 parameterizations also satisfy the X-Ray observational data by Steiner [88] and the recent observations of GW170817 maximum mass constraint of a stable non-rotating neutron star in the range  $2.01 \pm 0.04 - 2.16 \pm 0.03 M_{\odot}$  [92]. The hybrid EOSs obtained with the NJL model also satisfy astrophysical constraints on the maximum mass of a neutron star from PSR J1614-2230 [19]. The value of dimensionless tidal deformability ( $\Lambda_{1.4}$ ) calculated by employing the EOSs DOPS2, DOPS3, DOPS2Q, and DOPS3Q is found to be in the range 527.3 - 563.2 which is consistent with the waveform models analysis of GW170817 [17]. The value of ( $\Lambda_{1.4}$ ) calculated with EOSs DOPS1 and DOPS1Q is 627.37 and 637 which is consistent with the constraint on  $\Lambda_{1.4}$  obtained using Bayesian analysis [95].

## ACKNOWLEDGMENTS

Virender Thakur is highly thankful to Himachal Pradesh University and DST-INSPIRE for providing computational facility and financial assistance (Junior/Senior Research Fellowship).

- 
- [1] H. T. Cromartie, E. Fonseca, S. M. Ransom, P. B. Demorest, Z. Arzoumanian, H. Blumer, P. R. Brook, M. E. DeCesar, T. Dolch, J. A. Ellis, R. D. Ferdman, E. C. Ferrara, N. Garver-Daniels, P. A. Gentile, M. L. Jones, M. T. Lam, D. R. Lorimer, R. S. Lynch, M. A. McLaughlin, C. Ng, D. J. Nice, T. T. Pennucci, R. Spiewak, I. H. Stairs, K. Stovall, J. K. Swiggum, and W. W. Zhu, *Nature Astronomy* **4**, 72 (2020).
- [2] M. C. Miller, F. K. Lamb, A. J. Dittmann, S. Bogdanov, Z. Arzoumanian, K. C. Gendreau, S. Guil-

- lot, A. K. Harding, W. C. G. Ho, J. M. Lattimer, R. M. Ludlam, S. Mahmoodifar, S. M. Morsink, P. S. Ray, T. E. Strohmayer, K. S. Wood, T. Enoto, R. Foster, T. Okajima, G. Prigozhin, and Y. Soong, *The Astrophysical Journal* **887**, L24 (2019).
- [3] T. E. Riley, A. L. Watts, S. Bogdanov, P. S. Ray, R. M. Ludlam, S. Guillot, Z. Arzoumanian, C. L. Baker, A. V. Bilous, D. Chakrabarty, K. C. Gendreau, A. K. Harding, W. C. G. Ho, J. M. Lattimer, S. M. Morsink, and T. E. Strohmayer, **887**, L21 (2019).

- [4] S. K. Dhiman, R. Kumar, and B. K. Agrawal, *Phys. Rev. C* **76**, 045801 (2007).
- [5] F. Özel and P. Freire, *Annu. Rev. Astron. Astrophys.* **54**, 401 (2016).
- [6] M. Oertel, M. Hempel, T. Klähn, and S. Typel, *Rev. Mod. Phys.* **89**, 015007 (2017).
- [7] E. Annala, T. Gorda, A. Kurkela, and A. Vuorinen, *Phys. Rev. Lett.* **120**, 172703 (2018).
- [8] D. E. Alvarez-Castillo, D. B. Blaschke, A. G. Grunfeld, and V. P. Pagura, *Phys. Rev. D* **99**, 063010 (2019).
- [9] E. Witten, *Phys. Rev. D* **30**, 272 (1984).
- [10] E. Farhi and R. L. Jaffe, *Phys. Rev. D* **30**, 2379 (1984).
- [11] P. Haensel, J. L. Zdunik, and R. Schaeffer, *Astron. Astrophys.* **160**, 121 (1986).
- [12] C. Alcock, E. Farhi, and A. Olinto, *Astrophys. J.* **310**, 261 (1986).
- [13] J. M. Lattimer and M. Prakash, *Science* **304**, 536 (2004).
- [14] P. Haensel, A. Y. Potekhin, and D. G. Yakovlev, *Neutron stars 1: Equation of state and structure*, Vol. 326 (Springer Science & Business Media, 2007).
- [15] J. M. Lattimer, *Gen. Rel. Grav.* **46**, 1713 (2014).
- [16] G. Baym, T. Hatsuda, T. Kojo, P. D. Powell, Y. Song, and T. Takatsuka, *Rep. Prog. Phys.* **81**, 056902 (2018).
- [17] B. P. Abbott, R. Abbott, T. D. Abbott, F. Acernese, K. Ackley, C. Adams, T. Adams, P. Addesso, R. X. Adhikari, V. B. Adya, *et al.*, *Phys. Rev. Lett.* **121**, 161101 (2018).
- [18] B. P. Abbott, R. Abbott, T. D. Abbott, F. Acernese, K. Ackley, C. Adams, T. Adams, P. Addesso, R. X. Adhikari, V. B. Adya, *et al.*, *Phys. Rev. X* **9**, 011001 (2019).
- [19] P. B. Demorest, T. Pennucci, S. M. Ransom, M. S. E. Roberts, and J. W. T. Hessels, *nature* **467**, 1081 (2010).
- [20] J. Antoniadis, P. C. C. Freire, N. Wex, T. M. Tauris, R. S. Lynch, M. H. van Kerkwijk, M. Kramer, C. Bassa, V. S. Dhillon, T. Driebe, *et al.*, *Science* **340**, 1233232 (2013).
- [21] Z. Arzoumanian, A. Brazier, S. Burke-Spolaor, S. Chamberlain, S. Chatterjee, B. Christy, J. M. Cordes, N. J. Cornish, F. Crawford, H. T. Cromartie, *et al.*, *Astrophys. J. Suppl. S.* **235**, 37 (2018).
- [22] G. Raaijmakers, T. E. Riley, A. L. Watts, S. K. Greif, S. M. Morsink, K. Hebeler, A. Schwenk, T. Hinderer, S. Nissanke, S. Guillot, Z. Arzoumanian, S. Bogdanov, D. Chakrabarty, K. C. Gendreau, W. C. G. Ho, J. M. Lattimer, R. M. Ludlam, and M. T. Wolff, *The Astrophysical Journal* **887**, L22 (2019).
- [23] D. J. Champion, S. M. Ransom, P. Lazarus, F. Camilo, C. Bassa, V. M. Kaspi, D. J. Nice, P. C. C. Freire, I. H. Stairs, J. van Leeuwen, B. W. Stappers, J. M. Cordes, J. W. T. Hessels, D. R. Lorimer, Z. Arzoumanian, D. C. Backer, N. D. R. Bhat, S. Chatterjee, I. Cognard, J. S. Deneva, C.-A. Faucher-Giguère, B. M. Gaensler, J. Han, F. A. Jenet, L. Kasian, V. I. Kondratiev, M. Kramer, J. Lazio, M. A. McLaughlin, A. Venkataraman, and W. Vlemmings, *Science* **320**, 1309 (2008).
- [24] A. A. Abdo, M. Ackermann, M. Ajello, A. Allafort, E. Antolini, W. Atwood, M. Axelsson, L. Baldini, J. Ballet, G. Barbiellini, *et al.*, *Astrophys. J. Suppl. S.* **188**, 405 (2010).
- [25] L. Guillemot, P. Freire, I. Cognard, T. Johnson, Y. Takahashi, J. Kataoka, G. Desvignes, F. Camilo, E. Ferrara, A. Harding, *et al.*, *Mon. Not. R. astro. Soc.* **422**, 1294 (2012).
- [26] E. Fonseca, T. T. Pennucci, J. A. Ellis, I. H. Stairs, D. J. Nice, S. M. Ransom, P. B. Demorest, Z. Arzoumanian, K. Crowter, T. Dolch, *et al.*, *Astrophys. J.* **832**, 167 (2016).
- [27] G. Burgio, M. Baldo, P. Sahu, and H.-J. Schulze, *Physical Review C* **66**, 025802 (2002).
- [28] B. Sharma, P. Panda, and S. Patra, *Physical Review C* **75**, 035808 (2007).
- [29] G. B. Alaverdyan, *Research in Astronomy and Astrophysics* **10**, 1255 (2010).
- [30] P. Jaikumar, S. Reddy, and A. W. Steiner, *Physical review letters* **96**, 041101 (2006).
- [31] M. G. Alford, S. Han, M. Prakash, *et al.*, *Physical Review D* **88**, 083013 (2013).
- [32] Y. Nambu and G. Jona-Lasinio, *Physical review* **122**, 345 (1961).
- [33] Y. Nambu and G. Jona-Lasinio, *Physical review* **124**, 246 (1961).
- [34] K. Kikkawa, *Progress of Theoretical Physics* **56**, 947 (1976).
- [35] T. Eguchi, *Physical Review D* **14**, 2755 (1976).
- [36] M. Buballa, *Physics Reports* **407**, 205 (2005).
- [37] P. Rehberg, S. Klevansky, and J. Hüfner, *Physical Review C* **53**, 410 (1996).
- [38] I. F. Ranea-Sandoval, M. G. Orsaria, G. Malfatti, D. Curin, M. Mariani, G. A. Contrera, and O. M. Guilerá, *Symmetry* **11**, 425 (2019).
- [39] M. Alford and A. Sedrakian, *Physical review letters* **119**, 161104 (2017).
- [40] J. J. Li, A. Sedrakian, and M. Alford, *Physical Review D* **101**, 063022 (2020).
- [41] M. Alford, M. Braby, M. Paris, and S. Reddy, *Astrophys. J.* **629**, 969 (2005).
- [42] B. K. Agrawal and S. K. Dhiman, *Phys. Rev. D* **79**, 103006 (2009).
- [43] E.-P. Zhou, X. Zhou, and A. Li, *Phys. Rev. D* **97**, 083015 (2018).
- [44] D. P. Menezes, C. Providência, and D. Melrose, *J. Phys. G Nucl. Part. Phys.* **32**, 1081 (2006).
- [45] D. B. Blaschke, D. G. Dumm, A. G. Grunfeld, T. Klähn, and N. N. Scoccola, *Phys. Rev. C* **75**, 065804 (2007).
- [46] M. G. Alford, S. Han, and M. Prakash, *Phys. Rev. D* **88**, 083013 (2013).
- [47] M. Wang, G. Audi, F. Kondev, W. Huang, S. Naimi, and X. Xu, *Chin. Phys. C* **41**, 030003 (2017).
- [48] N. K. Glendenning, *Phys. Rev. D* **46**, 1274 (1992).
- [49] N. K. Glendenning, Springer-Verlag, New York (2000).
- [50] R. J. Furnstahl, *Nucl. Phys. A* **706**, 85 (2002).
- [51] T. Sil, M. Centelles, X. Vinas, and J. Piekarewicz, *Phys. Rev. C* **71**, 045502 (2005).
- [52] H. Mueller and B. D. Serot, *Nucl. Phys. A* **606**, 508 (1996).
- [53] R. Kumar, B. K. Agrawal, and S. K. Dhiman, *Phys. Rev. C* **74**, 034323 (2006).
- [54] M. Buballa, *Rep* **407**, 205 (2005).
- [55] H. Liu, J. Xu, L.-W. Chen, and K.-J. Sun, *Physical Review D* **94**, 065032 (2016).
- [56] N. Bratovic, T. Hatsuda, and W. Weise, *Physics Letters B* **719**, 131 (2013).
- [57] M. Lutz, S. Klimt, and W. Weise, *Nuclear Physics A* **542**, 521 (1992).
- [58] M. Frank, M. Buballa, and M. Oertel, *Physics Letters B* **562**, 221 (2003).

- [59] S. N. Zhang and et al.(eXTP Collaboration), Proc. of SPIE-Int. Soc. Opt. Eng. **9905**, 914420 (2014).
- [60] M. Alford, K. Rajagopal, S. Reddy, and F. Wilczek, Phys. Rev. D **64**, 074017 (2001).
- [61] N. Yasutake, R. Łastowiecki, S. Benić, D. Blaschke, T. Maruyama, and T. Tatsumi, Phys. Rev. C **89**, 065803 (2014).
- [62] T. Maruyama, S. Chiba, H.-J. Schulze, and T. Tatsumi, Phys. Rev. D **76**, 123015 (2007).
- [63] M. Favata, Phys. Rev. Lett. **112**, 101101 (2014).
- [64] L. Wade, J. D. E. Creighton, E. Ochsner, B. D. Lackey, B. F. Farr, T. B. Littenberg, and V. Raymond, Phys. Rev. D **89**, 103012 (2014).
- [65] T. Hinderer, Astrophys. J. **677**, 1216 (2008).
- [66] T. Hinderer, Astrophys. J. **697**, 964 (2009).
- [67] T. Hinderer, B. D. Lackey, R. N. Lang, and J. S. Read, Phys. Rev. D **81**, 123016 (2010).
- [68] T. Damour and A. Nagar, Phys. Rev. D. **81**, 084016 (2010).
- [69] M. Dutra, O. Lourenço, S. S. Avancini, B. V. Carlson, A. Delfino, D. P. Menezes, C. Providência, S. Typel, and J. R. Stone, Phys. Rev. C **90**, 055203 (2014).
- [70] M. Dutra, O. Lourenço, and D. P. Menezes, Phys. Rev. C **93**, 025806 (2016).
- [71] M. Fortin, C. Providência, A. R. Raduta, F. Gulminelli, J. L. Zdunik, P. Haensel, and M. Bejger, Phys. Rev. C **94**, 035804 (2016).
- [72] C. J. Horowitz and J. Piekarewicz, Phys. Rev. Lett. **86**, 5647 (2001).
- [73] O. Lourenço, M. Dutra, C. H. Lenzi, C. V. Flores, and D. P. Menezes, Phys. Rev. C **99**, 045202 (2019).
- [74] T. Bürvenich, D. Madland, and P.-G. Reinhard, Nuclear Physics A **744**, 92 (2004).
- [75] S. Kirkpatrick, Journal of statistical physics **34**, 975 (1984).
- [76] L.-W. Chen, C. M. Ko, and B.-A. Li, Phys. Rev. C **72**, 064309 (2005).
- [77] F. J. Fattoyev, C. J. Horowitz, J. Piekarewicz, and B. Reed, Phys. Rev. C **102**, 065805 (2020).
- [78] G. Lalazissis, J. König, and P. Ring, Physical Review C **55**, 540 (1997).
- [79] W.-C. Chen and J. Piekarewicz, Physics Letters B **748**, 284 (2015).
- [80] B. Kumar, S. K. Patra, and B. K. Agrawal, Phys. Rev. C **97**, 045806 (2018).
- [81] R. Furnstahl, B. D. Serot, and H.-B. Tang, Nucl. Phys. A **615**, 441 (1997).
- [82] B.-A. Li and X. Han, Physics Letters B **727**, 276 (2013).
- [83] G. Colo, U. Garg, and H. Sagawa, The European Physical Journal A **50**, 1 (2014).
- [84] J. Piekarewicz, The European Physical Journal A **50**, 1 (2014).
- [85] P. Danielewicz, Science **298**, 1592 (2002).
- [86] G. Baym, C. Pethick, and P. Sutherland, Astrophys. J. **170**, 299 (1971).
- [87] S. Weinberg, (1972).
- [88] A. Steiner, J. Lattimer, and E. Brown, J **722**, 33 (2010).
- [89] J. Nattila, A. W. Steiner, J. J. E. Kajava, V. F. Suleimanov, and J. Poutanen, Astron. Astrophys. **591**, A25 (2016).
- [90] R. Abbott, T. Abbott, S. Abraham, F. Acernese, K. Ackley, C. Adams, R. Adhikari, V. Adya, C. Affeldt, M. Agathos, *et al.*, The Astrophysical Journal Letters **896**, L44 (2020).
- [91] T. E. Riley, A. L. Watts, P. S. Ray, S. Bogdanov, S. Guillot, S. M. Morsink, A. V. Bilous, Z. Arzoumanian, D. Choudhury, J. S. Deneva, *et al.*, The Astrophysical Journal Letters **918**, L27 (2021).
- [92] L. Rezzolla, E. R. Most, and L. R. Weih, Astrophys. J. Lett. **852**, L25 (2018).
- [93] M. Miller, F. Lamb, A. Dittmann, S. Bogdanov, Z. Arzoumanian, K. Gendreau, S. Guillot, W. Ho, J. Lattimer, M. Loewenstein, *et al.*, The Astrophysical Journal Letters **918**, L28 (2021).
- [94] B. P. Abbott, R. Abbott, T. D. Abbott, F. Acernese, K. Ackley, C. Adams, T. Adams, P. Addesso, R. X. Adhikari, V. B. Adya, *et al.*, Phys. Rev. Lett. **119**, 161101 (2017).
- [95] Y. Li, H. Chen, D. Wen, and J. Zhang, The European Physical Journal A **57**, 1 (2021).
- [96] P.-C. Chu, B. Wang, H.-Y. Ma, Y.-M. Dong, S.-L. Chang, C.-H. Zheng, J.-T. Liu, and X.-M. Zhang, Physical Review D **93**, 094032 (2016).
- [97] J. Dobaczewski, W. Nazarewicz, and P. Reinhard, Journal of Physics G: Nuclear and Particle Physics **41**, 074001 (2014).
- [98] S. Abrahamyan, Z. Ahmed, H. Albataineh, K. Aniol, D. Armstrong, W. Armstrong, T. Averett, B. Babineau, A. Barbieri, V. Bellini, *et al.*, Physical review letters **108**, 112502 (2012).
- [99] J. Piekarewicz, Physical Review C **69**, 041301 (2004).